Improving thermal resistance in III-nitride blue and UV vertical-cavity surface-emitting lasers

Research Article Vol. 33, No. 16 / 11 Aug 2025 / Optics Express 34242
Optics EXPRESS

Improving thermal resistance in III-nitride blue and UV vertical-cavity surface-emitting lasers

LARS PERSSON,[1,*] GIULIA CARDINALI,[2] JOACHIM CIERS,[1] AND ÅSA HAGLUND[1]

[1]Department of Microtechnology and Nanoscience, Chalmers University of Technology, Gothenburg 41296, Sweden
[2]Institute of Solid State Physics, Technische Universität Berlin, 10623 Berlin, Germany
[*]lars.persson@chalmers.se

Abstract: Different mirror concepts are being explored in parallel for III-N vertical-cavity surface-emitting lasers (VCSELs), each with their own pros and cons. A general belief is that epitaxial distributed Bragg reflectors (DBRs) offer a VCSEL with superior thermal performance compared to all-dielectric DBRs. We here show that this is not the case for GaN-based VCSELs designed for 440 nm emission with cavity lengths $\geq 10\lambda$ due to a laterally dominated heat flow caused by the high thermal conductivity of GaN cavity material in contrast to the lower thermally conductive DBRs. If the same cavity design that is used for blue GaN VCSELs is applied to ultraviolet-C (UVC) AlGaN-VCSELs this will lead to detrimentally high internal temperatures (up to 370°C) due to the very low thermal conductivity of AlGaN which would prevent lasing. Increasing the cavity length to 30λ reduces the thermal resistance from 4400 K/W to 2600 K/W, but this is not enough. To drastically lower the internal temperature, we propose adding 300 nm AlN spacer layers to the AlGaN cavity, which reduces thermal resistance to 1100 K/W, which is similar to that of blue VCSELs. The low thermal resistance of this design shows promise for realizing electrically injected, continuous-wave AlGaN-based UVC VCSELs.

1. Introduction

Blue-emitting GaN-based vertical-cavity surface-emitting lasers (VCSELs) are promising for a wide range of applications due to their compact size, low threshold currents and 2D-array compatibility. These devices are particularly well-suited for advanced display technologies, including laser projectors, augmented reality systems, and retinal scanning displays. In automotive lighting, blue VCSELs combined with phosphors could enable adaptive headlights with dynamic beam shaping for enhanced visibility and safety [1,2]. Moreover, the high modulation speed of VCSELs at low drive currents, combined with the low absorption of blue light in water, makes blue VCSELs well-suited for underwater optical communication [3]. GaN-based VCSELs emitting in the blue wavelength region have been successfully demonstrated under continuous-wave (CW) electrical injection [4–11]. The internal temperature is a key factor limiting the VCSEL performance, making effective thermal management essential. In VCSELs, elevated internal temperatures lead to detrimental effects like detuning, a decrease in the gain peak and an increased leakage current [12,13], all of which conspire to increase the threshold current and lower the optical output power. This, in turn, exacerbates the temperature rise due to Joule heating and non-radiative recombination, creating a self-heating effect that further degrades device performance. Recent simulation studies have explored ways to reduce the thermal resistance of blue-emitting GaN-based VCSELs [14,15]. One promising approach is to increase the cavity length [14,15], which has been experimentally demonstrated by Kuramoto et al. [5], who fabricated 5λ and 10λ GaN-based VCSELs with a hybrid distributed Bragg reflector (DBR)

#567523 https://doi.org/10.1364/OE.567523
Journal © 2025 Received 13 May 2025; revised 4 Jul 2025; accepted 22 Jul 2025; published 4 Aug 2025

Optics EXPRESS

design, combining one epitaxial and one dielectric DBR. Their results showed a significant reduction in thermal resistance from 1100 K/W for the 5λ device to 710 K/W for the 10λ device, consistent with thermal simulations [14,15]. The reduced thermal resistance for the 10λ cavity delayed the onset of roll-over to higher currents allowing for a higher output power to be obtained. At roll-over, the internal temperature for both cavity lengths was calculated to be 150°C, when accounting for the wall-plug efficiency (WPE) of 8.9%.

Different mirror concepts, such as hybrid DBRs [4,5,10,16–24] and all-dielectric DBRs [25–35], are being explored in parallel for blue-emitting VCSELs, each with their own pros and cons. All-dielectric DBRs offer high refractive index contrast, resulting in a wide stop band and fewer mirror pairs ($\approx$ 10) to achieve high reflectivity (> 99 %), making them ideal from an optical standpoint. However, dielectric materials have low thermal conductivity ($\approx$ 1-3 W/mK), and an all-dielectric design requires substrate removal, which adds fabrication complexity. For blue VCSELs, the most common epitaxial mirror is an AlInN/GaN DBR. A general belief is that using a bottom epitaxial DBR, such as an AlInN/GaN DBR, offer a VCSEL with superior thermal performance compared to all-dielectric DBRs due to the high thermal conductivity of GaN (160 W/mK). However, since the thermal conductivity of AlInN is very low (9.4 W/mK), such a DBR has a poor vertical heat transport [36], only slightly better than that of a dielectric DBR. Additionally, the need for lattice matching between GaN and AlInN leads to a small refractive index contrast, resulting in a narrower stop band and requiring more mirror pairs ($\approx$ 40) to achieve the same reflectivity.

Pushing the emission wavelength into the ultraviolet-C (UVC) range (100–280 nm) would enable new applications, particularly in disinfection and sterilization. Since UVC light is strongly absorbed by atmospheric gases and does not naturally reach the Earth's surface, microorganisms have not developed resistance, making it highly effective at inactivating bacteria and viruses by damaging their nucleic acids [37]. However, achieving electrically injected AlGaN-based VCSELs for UVC emission remains a significant challenge. So far, all demonstrations of UV VCSELs have been optically pumped [38–40]. Some key obstacles to realizing electrically injected UVC VCSELs include overcoming the poor electrical conductivity of p-doped AlGaN [41,42] and obtaining high-reflectivity mirrors with a reflectivity exceeding 99% which is necessary for lasing [43]. So far, only dielectric DBRs have demonstrated such high reflectivities in the UVC and UVB spectral ranges [38,39,44] and all UVC and UVB VCSEL demonstrations have employed all-dielectric DBRs [38–40]. However, the use of dielectric DBRs, which have very low thermal conductivity, significantly impedes vertical heat dissipation in the VCSEL. From a thermal perspective, using AlN in the cavity would be ideal due to its high thermal conductivity of 210 W/mK [45], which facilitates lateral heat spreading. However, since the electrical conductivity of AlGaN decreases with increasing Al-content [41], a realistic UVC cavity would consist of AlGaN with around $70-75$% Al to keep optical absorption to a minimum around 275 nm. Unfortunately, AlGaN with this composition has an order of magnitude lower thermal conductivity compared with the binaries AlN and GaN [45,46]. The combination of using the ternary material AlGaN together with dielectric DBRs makes self-heating a significant obstacle to realize electrically injected AlGaN-based UV-VCSELs.

In this paper, we investigate the thermal properties of blue-emitting GaN-based VCSELs using both hybrid and all-dielectric DBR designs. Our thermal simulations reveal that for short cavities, the thermal resistance is higher for the all-dielectric design due to the insulating effect of the bottom DBR between the heat source and the heat sink. However, as the cavity length approaches 10λ, the thermal resistance difference between the hybrid and all-dielectric designs becomes marginal, with only a 5 % difference. This is because, in longer cavities, lateral heat flow becomes dominant. Increasing the cavity length also decreases the thermal resistance and we derive an analytical model that explains this behavior. For UVC VCSELs with an $Al_{0.75}Ga_{0.25}N$ cavity, we find that the thermal resistance is more than four times larger than that of blue VCSELs. Simply

Optics EXPRESS

extending the cavity length is not enough to reach a thermal resistance comparable to that of blue VCSELs. However, we propose an alternative solution that offers a promising path toward the development of electrically injected UVC VCSELs with manageable internal temperatures.

2. Thermal modeling

The steady-state thermal modeling was performed using a quasi three-dimensional (3D) finite element heat solver. The heat generated in the VCSEL structure is mainly transferred by conduction with only a small portion of the heat transferred by radiation and convection at the device-air interface. In our model we neglect the transfer of heat as radiation [15,47] and only account for conduction and convection

$$-\nabla \cdot (\kappa \nabla T) = p_{diss} \text{ where,}$$
$$\kappa \nabla T \cdot \hat{n} = h(T_{amb} - T) \text{ at the boundary,}$$

where κ is the thermal conductivity, T is the spatially varying temperature, p_{diss} is the heat source density, $\hat{n}$ is the normal unit vector at the air-device boundary, $h = 10\,\mathrm{W\,m^{-2}\,K^{-1}}$ is the heat transfer coefficient [47], and $T_{amb} = 20°\mathrm{C}$ is the ambient temperature. The bottom substrate is subject to Dirichlet's boundary condition with a fixed temperature of 20°C.

A useful concept to characterize the internal temperature of a VCSEL is the thermal resistance which is defined as the ratio between the increase in internal temperature to the total dissipated power [13]

$$R_{th} = \frac{\Delta T}{P_{diss}} = \frac{\partial \lambda / \partial P_{diss}}{\partial \lambda / \partial T_{sub}}, \tag{1}$$

where ΔT is the increase in the active region temperature relative to the ambient temperature. The latter is assumed to be 20°C in the simulations. The second equality in the equation shows that the internal temperature increase can be probed experimentally by measuring how the lasing wavelength shifts as a function of substrate temperature, $\partial\lambda/\partial T_{sub}$, and dissipated power, $\partial\lambda/\partial P_{diss}$.

The thermal resistance of a VCSEL structure is strongly related to the thermal conductivity of the materials in the cavity and in the surrounding DBRs. It is common for dielectric DBRs to exhibit a lower thermal conductivity as compared with epitaxially grown DBRs. However, the thermal conductivity of epitaxial DBRs greatly depends on alloy composition. Due to alloy scattering of phonons, the thermal conductivity in ternary AlInN, AlGaN and InGaN can be over one order of magnitude smaller than in the binary materials GaN, AlN and InN [46]. In our work, we have determined the thermal conductivity of alloyed materials using Adachi's model [46]

$$\frac{1}{\kappa_{A_xB_{1-x}C}} = \frac{x}{\kappa_{AC}} + \frac{(1-x)}{\kappa_{BC}} + x(1-x)\Gamma_{AB}, \tag{2}$$

where κ_{AC} and κ_{BC} are the binary thermal conductivities and the coefficient Γ_{AB} accounts for lattice disorder. Figure 1 shows the calculated thermal conductivities for the ternary compounds AlGaN, InGaN and AlInN with parameters taken from [45]. We extracted values from this figure in our modeling of blue- and UVC-emitting VCSELs and the exact values are summarized in Table 1 and 2. All simulations use constant values for the thermal conductivity at 300 K, without accounting for temperature dependence. This approach is consistent with previous thermal simulations of III-nitride VCSELs [14,15] and ensures that the observed differences in thermal resistance arise solely from changes in device geometry, rather than from temperature-dependent variations in material properties.

The thermal conductivity of multi-layered structures with thin layers, such as DBRs and multiple quantum wells (MQWs), can be replaced by a single layer with an effective lateral (κ_r)

Optics EXPRESS

Table 1. Vertical structure of the 10λ blue VCSEL with hybrid and all-dielectric mirror designs. EBL - electron blocking layer. CCL - current confinement layer. CSL - current spreading layer.

Layer	Material	Thickness (nm)	κ (W m^{-1} K^{-1})
Substrate (hybrid)	GaN	50000	160
Top-DBR (hybrid)	$Al_{0.8}In_{0.2}N$/GaN	3878.2 (49.90/44.69, 41 pairs)	κ_L = 84.2, κ_V = 9.4
Top-DBR (all-dielectric)	SiO_2/HfO_2	1273 (74.82/52.48, 10 pairs)	κ_L = 1.3, κ_V = 1.3
n-contact	n-GaN	1596	160
Active region	InGaN/GaN	35 (3/4, 5 pairs)	κ_L = 104.6, κ_V = 35.9
EBL	$Al_0.15Ga_0.85N$	20	20.79
p-contact	p-GaN	75	160
CCL	SiO_2	20	1.4
CSL	ITO	20	3
Spacer	HfO_2	52.48	1.2
Bottom-DBR	SiO_2/HfO_2	1400.3 (74.82/52.48, 11 pairs)	κ_L = 1.3, κ_V = 1.3
Bonding/p-contact metal	Au	500	315
Carrier substrate	Si	100000	130

Table 2. Vertical structure and material parameters for the 10λ all-dielectric UVC VCSEL. For the design with AlN spacers, the parameters *x* and *y* are varied between 0-300 nm and the two n-AlGaN layers are decreased to maintain a 10λ cavity. TJ - tunnel junction.

Layer	Material	Thickness (nm)	κ (W m^{-1} K^{-1})
Top-DBR	SiO_2/HfO_2	759 (45.65/30.25, 10 pairs)	κ_L = 1.3, κ_V = 1.3
Spacer	HfO_2	30.25	1.2
AlN spacer	AlN	0-x	210
n-side contact layer	n-$Al_{0.75}Ga_{0.25}N$	540.1 - $x n_{AlN}/n_{AlGaN}$	15.4
Barrier	$Al_{0.70}Ga_{0.20}N$	35	13.8
Active region	$Al_{0.3}Ga_{0.7}N/Al_{0.7}Ga_{0.3}N$	35 (2/5, 5 pairs)	κ_L = 13.8, κ_V = 13.8
Barrier	$Al_{0.70}Ga_{0.25}N$	40	13.8
Injection layer	p-$Al_{0.75}Ga_{0.25}N$	81.8	15.4
TJ	$Al_{0.75}Ga_{0.25}N$	10	15.4
p-side contact layer	n-$Al_{0.75}Ga_{0.25}N$	365.1 - $y n_{AlN}/n_{AlGaN}$	15.4
AlN spacer	AlN	0-y	210
Bottom-DBR	SiO_2/HfO_2	834.9 (45.65/30.25, 11 pairs)	κ_L = 1.3, κ_V = 1.3
Bonding/p-contact metal	Au	500	315
Substrate	AlN	100000	210

Optics EXPRESS

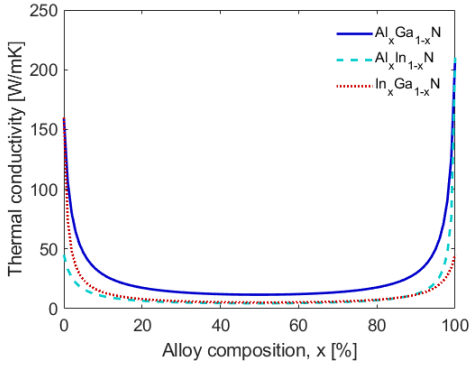

Fig. 1. Bulk thermal conductivity of III-nitride semiconductors used in the thermal modeling of blue and UVC VCSELs.

and vertical (κ_z) thermal conductivity [48,49].

$$\kappa_r = \frac{d_1\kappa_1 + d_2\kappa_2}{d_1 + d_2} \tag{3}$$

$$\kappa_z = \frac{d_1 + d_2}{d_1/\kappa_1 + d_2/\kappa_2} \tag{4}$$

where κ_1, κ_2 and d_1, d_2 are the thermal conductivity and the thickness of the alternating layers. As shown in Supplement 1 section S1, the heat conduction is stronger in the radial direction than in the vertical direction, with the ordering $\max(\kappa_1, \kappa_2) \geq \kappa_r \geq \kappa_z \geq \min(\kappa_1, \kappa_2)$. This approach with replacing a multi-layered stack with one effective layer has been used by multiple groups [15,36,47–49] and has the added benefit of reducing the number of mesh points, simulation time and memory requirement. The thermal conductivity may be further reduced from the expected bulk value due to finite size effects and scattering of phonons at interfaces if the distance between the layer interfaces is in the order of the phonon mean-free path [50]. Using the same approach as in [50] but for bulk GaN the estimated phonon mean-free path is around 30 nm, which is in the order of layer thicknesses in the DBR, see Table 1. Although this suggests that the thermal conductivity of the DBRs remain unaffected by size effects, it should be noted that this is a simple model using many assumptions, see Supplement 1 S2. However, we believe that neglecting finite-sized effects and interfacial thermal resistance is a reasonable approximation since thermal conduction through the DBR contributes only a small fraction and our thermal simulations successfully reproduce the experimentally measured thermal resistance and temperature of blue GaN-based VCSELs [5] as will be shown below.

Aside from the thermal conductivities of the materials in the VCSEL, the thermal resistance of the laser is also affected by the device's geometry and distribution of heat sources. Heat generation mainly occurs in the active region due to non-radiative recombination and in resistive layers due to Joule heating [13,51]. It is not straightforward to decide where to position these heat sources in the device simulations. In some papers, all of the heat sources are placed in the active region which is somewhat justified at threshold, but becomes increasingly inaccurate for currents exceeding the threshold current due to increasing resistive Joule heating. This approach may produce very high internal temperatures, especially for currents approaching roll-over, which is inconsistent with experimental observations [5]. A more realistic positioning of the heat sources can be obtained if the IV characteristics of the device are known, or can be approximated. The total dissipated power, P_{diss}, i.e. electrical input power minus optical output power, can be obtained from the WPE of the device and the drive current. Assuming that all the dissipated

Optics EXPRESS

power contributes to heat generation and that the voltage over the active region is clamped above threshold, we can separate P_{diss} into two components for currents $I \geq I_{th}$

$$\begin{aligned} P_{diss} &= (1 - \text{WPE})\Big[V_{th} + R_s(I - I_{th})\Big]I \\ &= (1 - \text{WPE})\Big[(V_{th} - R_s I_{th})I + R_s I^2\Big] = P_{MQW} + P_J, \end{aligned}$$

where I and V are the drive current and voltage, I_{th} and V_{th} are the threshold current and voltage, R_s is the series resistance of the device, P_{MQW} is the dissipated power in the active region and P_J is the dissipated power from Joule (resistive) heating. The wall-plug efficiency is a function of current; however, within a certain range (moderately above threshold and up to just before roll-over), its variation remains relatively small [5]. We assume that the p-side is much more resistive than the n-side of the GaN based VCSELs and therefore place all heat sources associated with Joule heating on the p-side. Depending on the operating conditions the fraction of dissipated power in the active region and p-side will vary. This implies that there will be a slight temperature dependence on the thermal resistance. We have chosen to ignore this and fixed the placement of heat sources based on a single operating point corresponding to the drive conditions at roll-over for a 10λ blue VCSEL from Kuramoto et al. [5]. For the 10λ blue VCSEL we have estimated a series resistance of $R_s = 85\ \Omega$ and at roll-over $I_{ro} = 28$ mA and $V_{ro} = 7.1$ V [5]. Using these values we find that 66% of the generated heat at roll-over is dissipated in the active region, and 34% as Joule heating in the p-side.

3. Thermal analysis of hybrid and all-dielectric DBRs in GaN VCSELs

Using the heat source placement described above, we are able to reproduce the experimentally determined thermal resistance and internal temperatures at roll-over, see Fig. 2, for the 5λ and 10λ hybrid GaN-VCSELs demonstrated by Kuramoto et al. [5]. The active region/aperture diameter of these VCSELs is 8 µm. Using the same epitaxial structure, but with an all-dielectric DBR design, see Table 1, we obtain a similar thermal resistance as for the GaN-VCSELs with a hybrid DBR design, see Fig. 3. As the cavity length is increased, the lateral heat flow becomes more dominant and there is an increasingly smaller difference in thermal resistance between the hybrid and all-dielectric designs despite the slightly higher thermal conductivity of the bottom AlInN/GaN mirror of the hybrid design. For a 10λ VCSEL, the all-dielectric scheme yields a thermal resistance (750 K/W) that is only 5% higher than the hybrid DBR design (710 K/W), thanks to the very efficient lateral heat flow provided by the highly thermally conductive GaN cavity. There is thus no significant thermal penalty for an all-dielectric DBR design.

In Fig. 2 it can be also observed that the thermal resistance varies inversely with cavity length, $R_{th} \propto 1/L_c$, as has been observed by others [14,15]. This dependence is valid in devices where lateral heat flow is dominant, see derivation in Supplement 1 S3. While this inverse scaling motivates the use of longer cavities to reduce thermal resistance, planar DBR designs are limited by diffraction losses. Alternative mirror configurations, such as curved DBRs, allow for significantly longer cavities without introducing large diffraction losses [52], and the reduction in thermal resistance using such cavities is estimated in Supplement 1 section S4.

Since the thermal conductivity of both the epitaxial and the dielectric DBRs are much lower than that of the GaN cavity, see Table 1, heat dissipation is mainly lateral for these devices. Figure 3(b)) and d) shows the temperature profiles of the hybrid and all-dielectric GaN-based VCSEL designs at roll-over. This operating point, corresponding to a dissipated power of 181 mW, was chosen because it provides a realistic estimate of the internal temperature at the onset of device failure in GaN-based VCSELs. The heat flux, indicated by the length of the white arrows, clearly demonstrates dominant lateral heat flow. Given that the predominant heat flow is through the p-contact, its proximity to the heat sources is critical for obtaining a low thermal resistance.

Optics EXPRESS

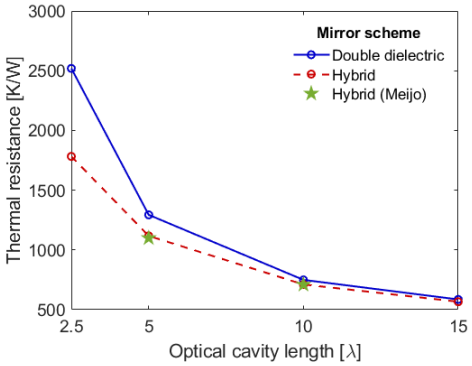

Fig. 2. Thermal resistance as a function of cavity length for a 440-nm GaN-VCSEL with an all-dielectric DBR (blue) and a hybrid DBR (red) design. Experimental data from Kuramoto et al. [5] (green) are included for comparison.

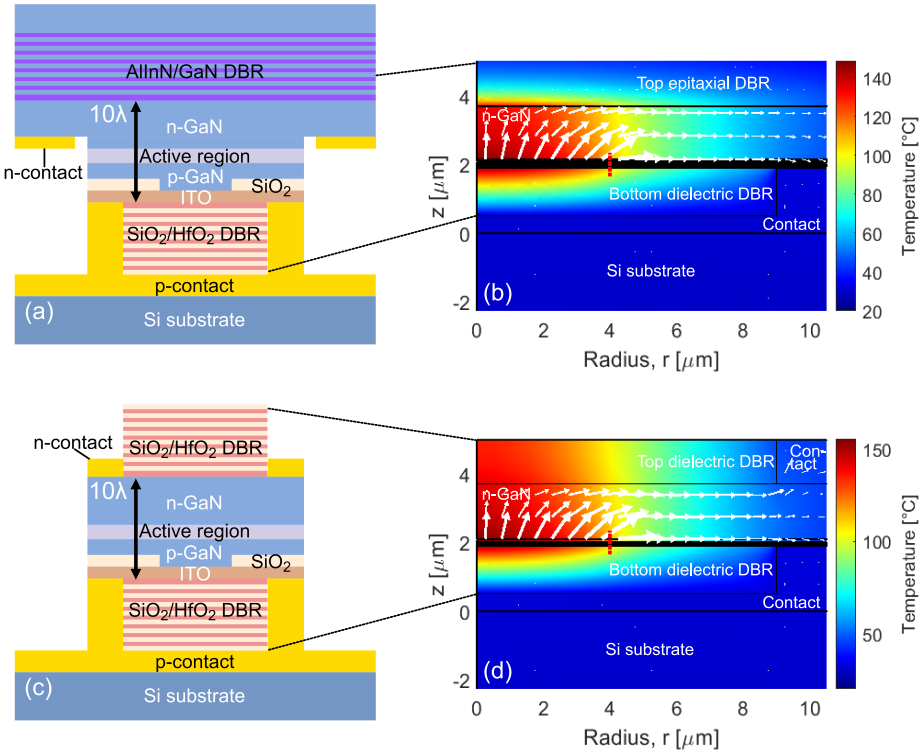

Fig. 3. Simulated steady-state temperature distribution in a 10λ blue VCSEL near roll-over with a total dissipated power of 181 mW. The length of the white arrows indicates the heat flux. A red dotted line has been inserted at r = 4 µm to indicate the extent of the current aperture. (a),(b) Blue VCSEL with a hybrid DBR design. The excellent thermal conductivity of GaN leads to an efficient lateral heat transport and at roll-over the internal temperature reaches 149°C (R_{th} = 710 K/W) in the active region. (c),(d) Blue VCSEL with an all-dielectric DBR design. Despite the addition of the thermally insulating bottom DBR, the excellent thermal conductivity of GaN leads to an efficient lateral heat transport as indicated by the white arrows. In this design a maximum internal temperature of 156°C (R_{th} = 750 K/W) is obtained in the active region.

Optics EXPRESS

In reality, the p-contact cannot be placed arbitrarily close to the active region due to alignment tolerances in the fabrication of the aperture, and to account for that we have assumed a bottom p-contact diameter of 18 µm in our simulations (i.e., a radial distance of 5 µm away from the edge of the aperture, see Fig. 3). More details on the positioning of the p-contact and thermal simulations of its impact on the thermal resistance can be found in Supplement 1 S5.

4. Thermal design considerations for UVC VCSELs

In UVC VCSELs the ternary material AlGaN is used instead of the highly thermally conductive GaN that can be used in blue VCSELs, which severely limits the lateral heat flow. We are here investigating the expected internal temperatures for a 10λ (1.2 µm) $Al_{0.75}Ga_{0.25}N$ UVC-VCSEL with all-dielectric DBRs, as shown in Fig. 4, under estimated steady-state conditions that could occur in electrical CW operated devices. The all-dielectric DBR configuration is realized by flip-chip bonding the cavity with the p-side facing downward in a similar way as for a blue VCSEL with all-dielectric DBRs. Given the poor p-type electrical conductivity of the high-Al containing AlGaN used in the cavity, we believe that using a tunnel junction (TJ) is the most effective approach to enable both hole injection and lateral current spreading, since it allows for using conductive n-AlGaN for current spreading on the p-side [42]. A tunnel junction design is therefore assumed for the UVC VCSELs. Details of the VCSEL layers and thermal conductivities used in the simulations are given in Table 2.

In addition to the poor thermal conductivity of AlGaN, UV VCSELs are expected to have higher thresholds. For the simulations done here we have assumed a dissipated power of 80 mW which is four times the dissipated power for a 10λ blue VCSEL at threshold. We obtain a thermal resistance of 4400 K/W, and an internal temperature of 370°C for a dissipated power of 80 mW. From the heat map in Fig. 4(b)) we can see that due to the poor thermal conductivity of $Al_{0.75}Ga_{0.25}N$, a significant portion of the heat flow, as indicated by the white arrows, is dissipated through the bottom dielectric DBR. This is a testament to the poor heat dissipation in this UVC VCSEL design. Experimental data show that high-performance blue GaN-based VCSELs experience roll-over at internal temperatures around 150°C [5], though this may vary with device detuning [42,53]. Therefore, we expect that this UVC VCSEL design, with an internal temperature of 370°C, would undergo roll-over before reaching the lasing threshold, effectively preventing lasing.

For blue VCSELs, increasing the cavity length reduces the thermal resistance. This trend also holds for the UVC VCSEL studied here, see Fig. 5(a)), although the effect is less pronounced due to the low thermal conductivity of $Al_{0.75}Ga_{0.25}N$. Increasing the cavity length from 10λ to 30λ reduces thermal resistance from 4400 to 2580 K/W. However, with a 30λ $Al_{0.75}Ga_{0.25}N$ cavity, the internal temperature reaches 230°C, still significantly higher than the 150°C at which blue VCSELs experience roll-over. Additionally, growing a 30λ $Al_{0.75}Ga_{0.25}N$ cavity on an AlN template could be challenging. The strain may cause the AlGaN cavity to relax, leading to the formation of defects. Using a long cavity with planar mirrors may also result in significant diffraction losses.

To reduce the internal temperature of the UVC VCSEL, we propose adding AlN layers with high thermal conductivity (210 W/mK) on both the n- and p-side of the cavity, see Fig. 4(c)) and Table 2. To maintain compatibility with electrical injection, parts of the AlN must be etched away on both sides to form electrical contacts directly on the n-$Al_{0.75}Ga_{0.25}N$ layers. For a fair comparison, the thickness of the $Al_{0.75}Ga_{0.25}N$ layers is reduced to keep the cavity's optical thickness at 10λ, as in the original design without AlN spacers. Our thermal simulations show that adding 300 nm thick AlN layers on both sides reduces the internal temperature from 370°C to 110°C, while decreasing thermal resistance by over 70% (from 4400 K/W to 1140 K/W), see Fig. 4(d)). As shown in Fig. 4(d)), the AlN layers create two parallel thermal shunts, which aids in redistributing heat laterally. This bypasses the low thermal conductivity of $Al_{0.75}Ga_{0.25}N$ in

Optics EXPRESS

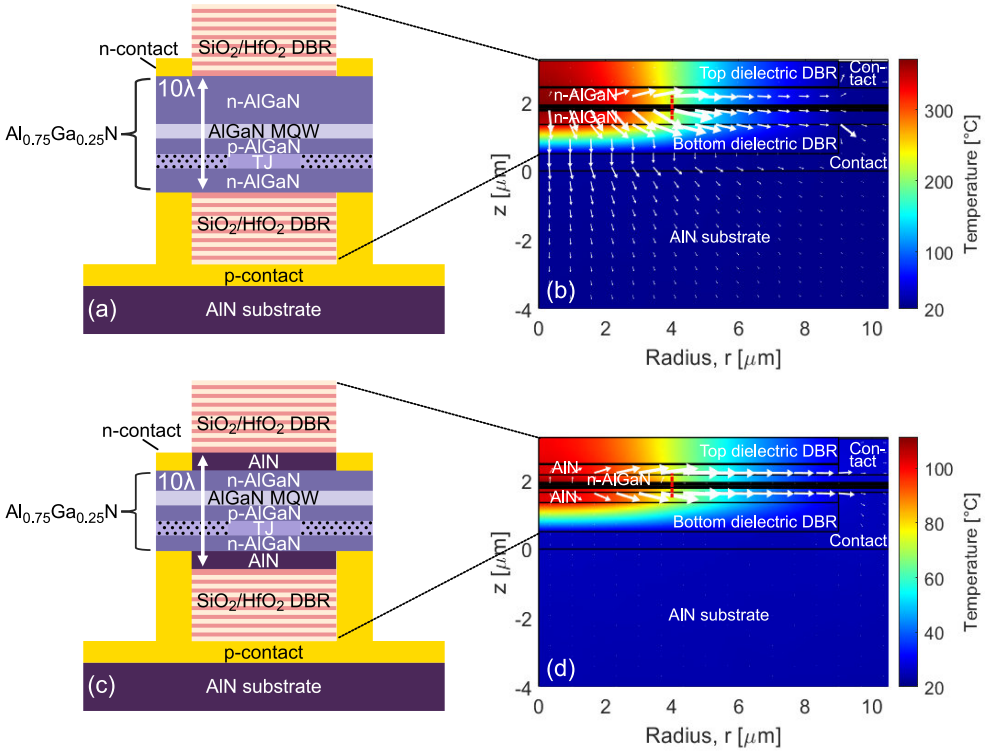

Fig. 4. Simulated steady-state temperature distribution in a 10λ UVC VCSEL near threshold with a total dissipated power of 80 mW. The white arrows indicate the heat flux. A red dotted line has been inserted at r = 4 µm to indicate the extent of the current aperture. (a),(b) Cavity consisting of $Al_{0.75}Ga_{0.25}N$. The poor thermal conductivity of AlGaN leads to an inefficient heat transfer from the active region resulting in a high temperature of 370°C (R_{th} = 4400 K/W) in the active region. (c),(d) Part of the n-AlGaN layer has been replaced by a 300-nm thick AlN-layer on both the n-side (top) and p-side (bottom) of the cavity. The excellent thermal conductivity of the AlN layers facilitates the lateral transport of heat as indicated by the white arrows. In this design a maximum internal temperature of 110°C (R_{th} = 1140 K/W) is reached in the active region.

Optics EXPRESS

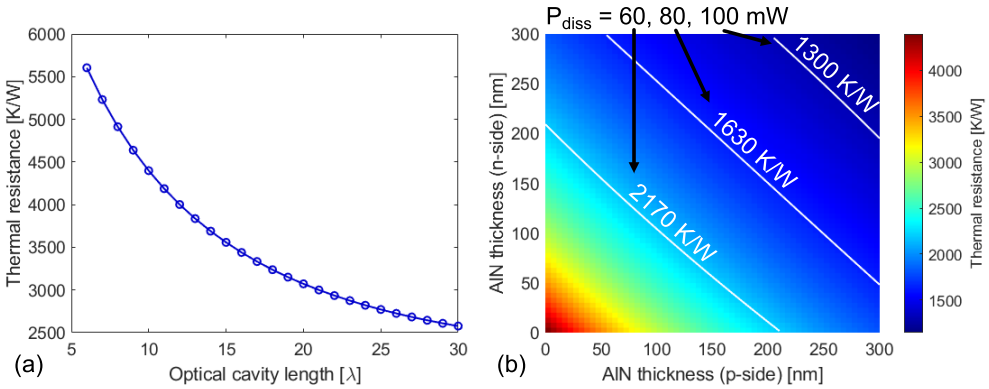

Fig. 5. (a) Thermal resistance for a UVC VCSEL, without AlN spacer layers, as a function of cavity length. The optical cavity length is varied by varying the n-side AlGaN thickness. (b) Thermal resistance for a 10-λ UVC VCSEL as a function of the n- and p-side AlN thicknesses. The optical cavity length of 10λ is maintained by decreasing the n- and p-side $Al_{0.75}Ga_{0.25}N$ thickness as the AlN thicknesses are increased. The white contour lines indicates the thermal resistance needed to produce a maximal internal temperature lower than 150°C for dissipated power levels of P_{diss}^{th} = 60, 80, and 100 mW.

the cavity, enhancing overall heat transport and lowering the internal temperature. We believe that this structure, with AlN spacers on either side of the $Al_{0.75}Ga_{0.25}N$ cavity, can be grown epitaxially on AlN templates without relaxing, as similar configurations have been realized for UVC LEDs [54]. Since the actual threshold current and voltage in future UVC VCSELs remain unknown, we have included contour lines in Fig. 5(b)) to indicate the required thermal resistance needed to produce an internal temperature below 150°C assuming three different power levels at threshold, P_{diss} = 60, 80, and 100 mW.

5. Conclusions

In conclusion, we have demonstrated that an all-dielectric design for blue GaN-based VCSELs does not result in a significant thermal penalty compared to a hybrid design. In VCSELs with thermally insulating DBRs, where lateral heat transport dominates, increasing the cavity length reduces the thermal resistance. When the aperture diameter is significantly larger than the cavity length, the steady-state temperature distribution becomes nearly homogeneous within a cylindrical volume defined by the aperture diameter and cavity length. In this scenario, increasing the cavity length expands the surface area available for radial heat diffusion, enhancing lateral heat dissipation and thereby reducing the overall thermal resistance.

We have also shown that applying the same cavity design principles used for blue GaN-based VCSELs to UVC $Al_{0.75}Ga_{0.25}N$-based VCSELs, the internal temperature becomes very high, up to 370°C (R_{th} = 4400 K/W). This high temperature will likely prevent lasing as GaN VCSELs experience roll-over effects at 150°C. To combat this issue, we propose incorporating 300 nm AlN spacers on both sides of the cavity to enhance lateral heat dissipation. This reduces thermal resistance from 4400 K/W to 1140 K/W for a 10λ cavity, lowering the internal temperature to 110°C—below the typical roll-over temperature of blue VCSELs. By lowering the thermal resistance, the device can sustain higher current densities before reaching thermal roll-over. This is expected to improve the chances of reaching threshold under CW operation and enable higher output power. Furthermore, reducing self-heating minimizes detuning between the gain peak and cavity resonance, which helps maintain a low threshold current and improves device stability. This approach shows great promise for the development of electrically driven UVC VCSELs.

Optics EXPRESS

Funding. H2020 European Research Council (865622); Vetenskapsrådet (2018-00295).

Acknowledgment. The project was financially supported by the European Research Council (ERC) under the European Union's Horizon 2020 research and innovation program (grant agreement no. 865622) and the Swedish Research Council (2018-00295).

Disclosures. The authors declare no conflicts of interest.

Data availability. The data that support the findings of this study are available from the corresponding author upon reasonable request.

Supplemental document. See Supplement 1 for supporting content.

References

1. S. Hoshino, Y. Kita, M. Uchida, *et al.*, "Challenges for the laser scanning headlamps to realize safe driving experience," in *Proceedings of the 12th International Symposium on Automotive Lighting; München Herbert Utz Verlag GmbH: München, Germany*, Vol. 17 (2017), pp. 299–305.
2. J. Hager, M. Seitz, C. Bemmer, *et al.*, "Handling 17w of scanning laser power–three years of exploration in the ilas project," in *Proceedings of the 12th International Symposium on Automotive Lighting; München Herbert Utz Verlag GmbH: München, Germany*, Vol. 17 (2017), pp. 271–280.
3. J. Baghdady, K. Miller, S. Osler, *et al.*, "Blue-light digital communication in underwater environments utilizing orbital angular momentum," in *Blue-light digital communication in underwater environments utilizing orbital angular momentum*, Vol. 9827 (SPIE, 2016), pp. 114–121.
4. R. Watanabe, K. Kobayashi, M. Yanagawa, *et al.*, "Over 20% wall plug efficiency of on-wafer GaN-based vertical-cavity surface-emitting laser," Appl. Phys. Lett. **124**(13), 131107 (2024).
5. M. Kuramoto, S. Kobayashi, T. Akagi, *et al.*, "High-output-power and high-temperature operation of blue GaN-based vertical-cavity surface-emitting laser," Appl. Phys. Express **11**(11), 112101 (2018).
6. K. Hayashi, T. Hamaguchi, J. A. Kearns, *et al.*, "Narrow Emission of Blue GaN-Based Vertical-Cavity Surface-Emitting Lasers With a Curved Mirror," IEEE Photonics J. **14**(4), 1–5 (2022).
7. K. Terao, H. Nagai, D. Morita, *et al.*, "Blue and green GaN-based vertical-cavity surface-emitting lasers with AlInN/GaN DBR," in *Gallium Nitride Materials and Devices XVI*, vol. 11686 (SPIE, 2021), pp. 116860E.
8. J. A. Kearns, J. Back, D. A. Cohen, *et al.*, "Demonstration of blue semipolar (2021) GaN-based vertical-cavity surface-emitting lasers," Opt. Express **27**(17), 23707–23713 (2019).
9. M. Kawaguchi, O. Imafuji, K. Nagamatsu, *et al.*, "Design and lasing characteristics of GaN vertical elongated cavity surface emitting lasers," *Gallium Nitride Materials and Devices IX* 8986 (SPIE, 2014), pp. 184–189.
10. T.-C. Lu, C.-C. Kao, H.-C. Kuo, *et al.*, "CW lasing of current injection blue GaN-based vertical cavity surface emitting laser," Appl. Phys. Lett. **92**(14), 141102 (2008).
11. R. Xu, Y. Mei, H. Xu, *et al.*, "Green Vertical-Cavity Surface-Emitting Lasers Based on Combination of Blue-Emitting Quantum Wells and Cavity-Enhanced Recombination," IEEE Trans. Electron Devices **65**(10), 4401–4406 (2018).
12. T.-C. Chang, S.-Y. Kuo, J.-T. Lian, *et al.*, "High-temperature operation of GaN-based vertical-cavity surface-emitting lasers," Appl. Phys. Express **10**(11), 112101 (2017).
13. S. F. Yu, *Analysis and Design of Vertical Cavity Surface Emitting Lasers* (John Wiley & Sons, 2003).
14. S. Mishkat-Ul-Masabih, J. Leonard, D. Cohen, *et al.*, "Techniques to reduce thermal resistance in flip-chip GaN-based VCSELs," Phys. Status Solidi A **214**(8), 1600819 (2017).
15. Y. Mei, R.-B. Xu, H. Xu, *et al.*, "A comparative study of thermal characteristics of GaN-based VCSELs with three different typical structures," Semicond. Sci. Technol. **33**(1), 015016 (2018).
16. T.-C. Lu, S.-W. Chen, T.-T. Wu, *et al.*, "Continuous wave operation of current injected GaN vertical cavity surface emitting lasers at room temperature," Appl. Phys. Lett. **97**(7), 071114 (2010).
17. T.-C. Lu, T.-T. Wu, S.-W. Chen, *et al.*, "Characteristics of Current-Injected GaN-Based Vertical-Cavity Surface-Emitting Lasers," IEEE J. Sel. Top. Quantum Electron. **17**(6), 1594–1602 (2011).
18. D. H. Hsieh, A. J. Tzou, T. S. Kao, *et al.*, "Improved carrier injection in GaN-based VCSEL via AlGaN/GaN multiple quantum barrier electron blocking layer," Opt. Express **23**(21), 27145–27151 (2015).
19. G. Cosendey, A. Castiglia, G. Rossbach, *et al.*, "Blue monolithic AlInN-based vertical cavity surface emitting laser diode on free-standing GaN substrate," Appl. Phys. Lett. **101**(15), 151113 (2012).
20. K. Matsui, Y. Kozuka, K. Ikeyama, *et al.*, "GaN-based vertical cavity surface emitting lasers with periodic gain structures," Jpn. J. Appl. Phys. **55**(5S), 05FJ08 (2016).
21. T. Furuta, K. Matsui, K. Horikawa, *et al.*, "Room-temperature CW operation of a nitride-based vertical-cavity surface-emitting laser using thick GaInN quantum wells," Jpn. J. Appl. Phys. **55**(5S), 05FJ11 (2016).
22. N. Hayashi, J. Ogimoto, K. Matsui, *et al.*, "A GaN-Based VCSEL with a Convex Structure for Optical Guiding," Physica Status Solidi (a) **215**(10), 1700648 (2018).
23. R. T. Elafandy, J. H. Kang, B. Li, *et al.*, "GaN blue vertical-cavity surface-emitting lasers using conductive nanoporous distributed Bragg reflectors," in *Light-Emitting Devices, Materials, and Applications XXV*, vol. 11706 (SPIE, 2021), pp. 135–142.

Optics EXPRESS

24. R. Iida, Y. Ueshima, S. Iwayama, *et al.*, "Aperture diameter dependences in GaN-based vertical-cavity surface-emitting lasers with nano-height cylindrical waveguide formed by BCl3 dry etching," Appl. Phys. Express **14**(1), 012003 (2021).
25. Y. Higuchi, K. Omae, H. Matsumura, *et al.*, "Room-Temperature CW Lasing of a GaN-Based Vertical-Cavity Surface-Emitting Laser by Current Injection," Appl. Phys. Express **1**, 121102 (2008).
26. K. Omae, Y. Higuchi, K. Nakagawa, *et al.*, "Improvement in Lasing Characteristics of GaN-based Vertical-Cavity Surface-Emitting Lasers Fabricated Using a GaN Substrate," Appl. Phys. Express **2**, 052101 (2009).
27. D. Kasahara, D. Morita, T. Kosugi, *et al.*, "Demonstration of Blue and Green GaN-Based Vertical-Cavity Surface-Emitting Lasers by Current Injection at Room Temperature," Appl. Phys. Express **4**(7), 072103 (2011).
28. T. Onishi, O. Imafuji, K. Nagamatsu, *et al.*, "Continuous Wave Operation of GaN Vertical Cavity Surface Emitting Lasers at Room Temperature," IEEE J. Quantum Electron. **48**(9), 1107–1112 (2012).
29. C. Holder, J. S. Speck, S. P. DenBaars, *et al.*, "Demonstration of Nonpolar GaN-Based Vertical-Cavity Surface-Emitting Lasers," Appl. Phys. Express **5**(9), 092104 (2012).
30. J. T. Leonard, E. C. Young, B. P. Yonkee, *et al.*, "Demonstration of a III-nitride vertical-cavity surface-emitting laser with a III-nitride tunnel junction intracavity contact," Appl. Phys. Lett. **107**(9), 091105 (2015).
31. J. T. Leonard, D. A. Cohen, B. P. Yonkee, *et al.*, "Nonpolar III-nitride vertical-cavity surface-emitting lasers incorporating an ion implanted aperture," Appl. Phys. Lett. **107**(1), 011102 (2015).
32. S. Izumi, N. Fuutagawa, T. Hamaguchi, *et al.*, "Room-temperature continuous-wave operation of GaN-based vertical-cavity surface-emitting lasers fabricated using epitaxial lateral overgrowth," Appl. Phys. Express **8**(6), 062702 (2015).
33. T. Hamaguchi, N. Fuutagawa, S. Izumi, *et al.*, "Milliwatt-class GaN-based blue vertical-cavity surface-emitting lasers fabricated by epitaxial lateral overgrowth," Physica Status Solidi (a) **213**(5), 1170–1176 (2016).
34. T. Hamaguchi, M. Tanaka, J. Mitomo, *et al.*, "Lateral optical confinement of GaN-based VCSEL using an atomically smooth monolithic curved mirror," Sci. Rep. **8**(1), 10350 (2018).
35. T. Hamaguchi, Y. Hoshina, K. Hayashi, *et al.*, "Room-temperature continuous-wave operation of green vertical-cavity surface-emitting lasers with a curved mirror fabricated on 2021 semi-polar GaN," Appl. Phys. Express **13**(4), 041002 (2020).
36. K. Mehta, Y.-S. Liu, J. Wang, *et al.*, "Thermal Design Considerations for III-N Vertical-Cavity Surface-Emitting Lasers Using Electro-Opto-Thermal Numerical Simulations," IEEE J. Quantum Electron. **55**(5), 1–8 (2019).
37. M. Kneissl, T.-Y. Seong, J. Han, *et al.*, "The emergence and prospects of deep-ultraviolet light-emitting diode technologies," Nat. Photonics **13**(4), 233–244 (2019).
38. F. Hjort, J. Enslin, M. Cobet, *et al.*, "A 310 nm Optically Pumped AlGaN Vertical-Cavity Surface-Emitting Laser," ACS Photonics **8**(1), 135–141 (2021).
39. Z. Zheng, Y. Mei, H. Long, *et al.*, "AlGaN-Based Deep Ultraviolet Vertical-Cavity Surface-Emitting Laser," IEEE Electron Device Lett. **42**(3), 375–378 (2021).
40. Z. Zheng, Y. Wang, J. Hoo, *et al.*, "High-quality AlGaN epitaxial structures and realization of UVC vertical-cavity surface-emitting lasers," Sci. China Mater. **66**(5), 1978–1988 (2023).
41. J. H. Park, D. Y. Kim, E. F. Schubert, *et al.*, "Fundamental Limitations of Wide-Bandgap Semiconductors for Light-Emitting Diodes," ACS Energy Lett. **3**(3), 655–662 (2018).
42. E. Torres, J. Ciers, M. A. Bergmann, *et al.*, "Ultraviolet-B Resonant-Cavity Light-Emitting Diodes with Tunnel Junctions and Dielectric Mirrors," ACS Photonics **11**(8), 2923–2929 (2024).
43. Å. Haglund, E. Hashemi, and J. Bengtsson, "Progress and challenges in electrically pumped GaN-based VCSELs," in *Semiconductor Lasers and Laser Dynamics VII*, Vol. 9892 (SPIE, 2016), pp. 161–180.
44. A. Yabutani, R. Hasegawa, R. Kondo, *et al.*, "Development of High-Reflectivity and Antireflection Dielectric Multilayer Mirrors for AlGaN-Based Ultraviolet-B Laser Diodes and their Device Applications," Physica Status Solidi (a) **220**(16), 2200831 (2023).
45. A. Filatova-Zalewska, Z. Litwicki, T. Suski, *et al.*, "Thermal conductivity of thin films of gallium nitride, doped with aluminium, measured with 3ω method," Solid State Sci. **101**, 106105 (2020).
46. S. Adachi, "Lattice thermal conductivity of group-IV and III–V semiconductor alloys," J. Appl. Phys. **102**(6), 063502 (2007).
47. H. K. Lee and J. S. Yu, "Thermal Analysis of InGaN/GaN Multiple Quantum Well Light Emitting Diodes with Different Mesa Sizes," Jpn. J. Appl. Phys. **49**(4S), 04DG11 (2010).
48. M. Osiński and W. Nakwaski, "Effective thermal conductivity analysis of 1.55 μm InGaAsP/InP vertical-cavity top-surface-emitting microlasers," Electron. Lett. **29**(11), 1015–1016 (1993).
49. J. Wang, I. Savidis, and E. G. Friedman, "Thermal analysis of oxide-confined VCSEL arrays," Microelectron. J. **42**(5), 820–825 (2011).
50. J. Piprek, T. Troger, B. Schroter, *et al.*, "Thermal conductivity reduction in GaAs-AlAs distributed Bragg reflectors," IEEE Photonics Technol. Lett. **10**(1), 81–83 (1998).
51. M. J. As'adi, K. Abbasian, D. Armaghan Bostanabad, *et al.*, "Thermal analysis of high-index-contrast grating (HCG)-based VCSEL," Optik **125**(15), 4017–4022 (2014).
52. T. Hamaguchi, "GaN-Based VCSELs with A Monolithic Curved Mirror: Challenges and Prospects," Photonics **10**(4), 470 (2023).

Optics EXPRESS

53. G. Cardinali, F. Hjort, N. Prokop, *et al.*, "Low-threshold AlGaN-based UVB VCSELs enabled by post-growth cavity detuning," Appl. Phys. Lett. **121**(10), 103501 (2022).
54. L. Guo, Y. Guo, J. Yang, *et al.*, "275 nm Deep Ultraviolet AlGaN-Based Micro-LED Arrays for Ultraviolet Communication," IEEE Photonics J. **14**(6), 1–8 (2022).